INFORMATION OF ELECTROMAGNETIC SCATTERING AND QUANTITATIVE REMOTE SENSING

电磁散射信息与定量遥感

金亚秋 著 Ya-Qiu Jin

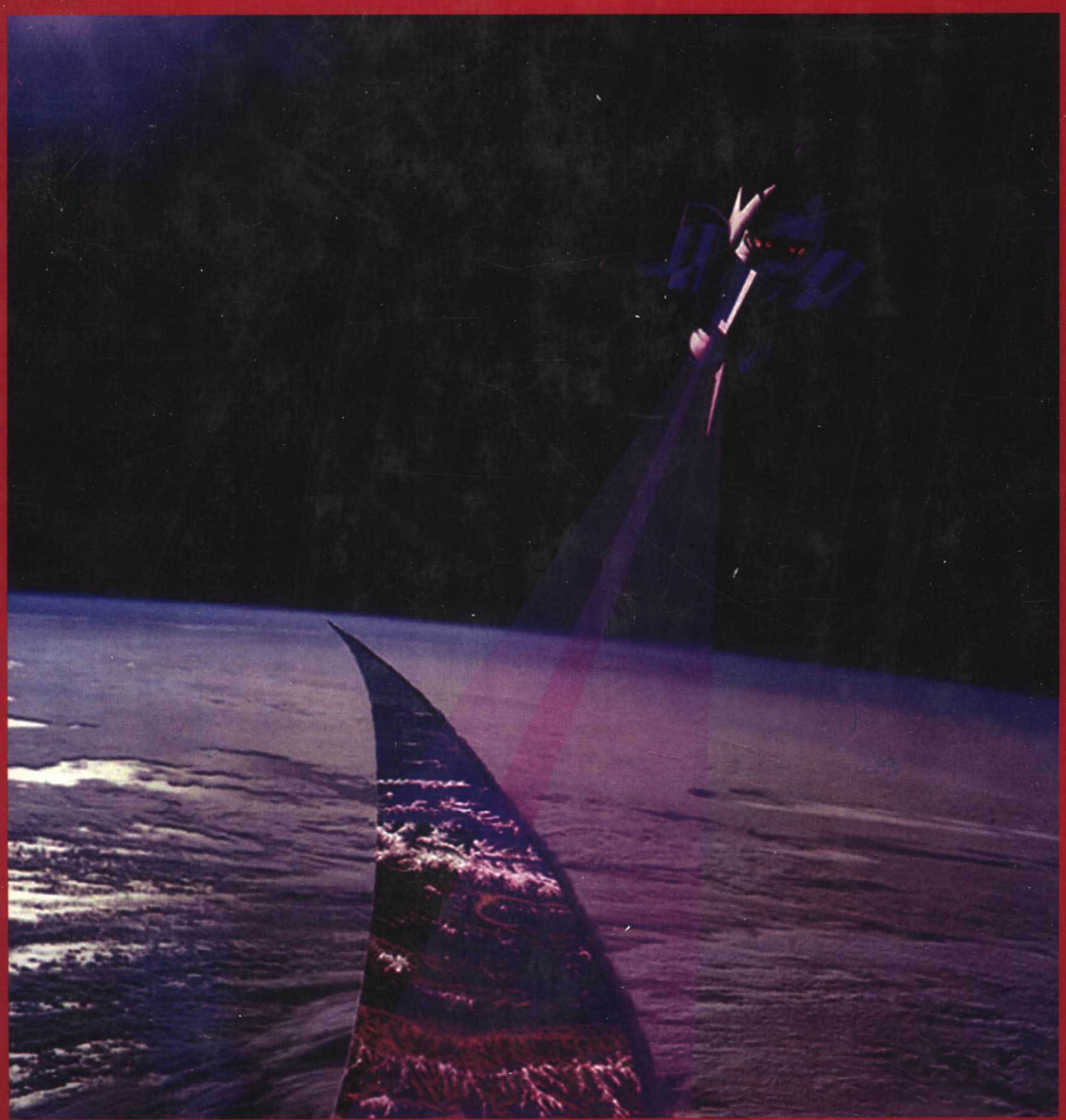

复旦大学出版社 Fudan University Press

电磁散射信息与定量遥感

Information of Electromagnetic Scattering and Quantitative Remote Sensing

金亚秋 著
Ya-Qiu Jin

复旦大学出版社
Fudan University Press

图书在版编目(CIP)数据

电磁散射信息与定量遥感/金亚秋著．—上海：复旦大学出版社，2000.6
ISBN 7-309-02520-2

Ⅰ．电… Ⅱ．金… Ⅲ．电磁波散射-遥感图像-图像解译-文集
Ⅳ．TP75-53

中国版本图书馆 CIP 数据核字(2000)第 18615 号

出版发行 复旦大学出版社
上海市国权路 579 号 200433
86-21-65102941(发行部) 86-21-65642892(编辑部)
fupnet@fudanpress.com http://www.fudanpress.com
经销 新华书店上海发行所
印刷 江苏丹阳市教育印刷厂
开本 890×1240 1/16
印张 29.25 插页 1
字数 465 千
版次 2000 年 6 月第一版 2000 年 6 月第一次印刷
定价 58.00 元

如有印装质量问题，请向复旦大学出版社发行部调换。

内容简介

本书选自作者及其合作者在1980-1999年期间发表的学术刊物论文，讨论了模拟自然环境的随机介质矢量辐射传输理论(VRT)、自然植被地表的全极化散射理论、随机粗糙面散射理论、空对地微波遥感建模与数值模拟、星载遥感数据验证与参数反演、复杂介质电磁散射理论与计算电磁学方法等诸多方面的一些前沿基础理论及其实际应用。

本书可作为无线电物理、地球信息科学、地球海洋大气空间遥感、应用物理等多学科科技工作者研究参考书和有关专业研究生对前沿课题研究的教学参考书。

Abstract

This book is collection of some journal publications by the author with his collaborators during 1980-1999. To develop theoretical simulation and inversion of microwave remote sensing, this book presents some advances on the theories of vector radiative transfer in random media, fully polarimetric scattering of canopy surfaces, and scattering from randomly rough surfaces. Theoretical modeling, numerical simulation, data validation and parameter retrievals for space-borne microwave remote sensing, and computational methods for scattering from complex objects are discussed.

This book can be an useful reference for scientists in the radiophysics, Earth sciences, especially in remote sensing of atmosphere, ocean and land surfaces, and applied physics. It can also be used as a textbook for graduate students to study some frontier topics in electromagnetic scattering and remote sensing.

前　言

本书由作者自 1980 年在美国麻省理工学院(MIT)攻读研究生至回国后在复旦大学任教的 20 年中与其合作者在国内外发表的学术论文选辑而成。本书汇总了模拟自然环境的随机介质矢量辐射传输理论、自然植被地表的全极化散射理论、随机粗糙面散射理论、空对地微波遥感建模与数值模拟、星载遥感数据验证与参数反演、复杂介质电磁散射理论与计算电磁学方法等诸多方面的研究成果。为便于国内外学术交流，选辑的论文大多为英文，国内外同行与研究生阅读不会有困难。

本书共分为六章，每章讨论一个课题。矢量辐射传输(VRT)理论是研究复杂介质中极化电磁波强度-Stokes 矢量多次散射与辐射传输的理论。第一章讨论了模拟非等温非均匀大气降水、海冰、多层植被、陆地土壤等自然介质的 VRT 理论，也讨论了各向异性介电强起伏随机介质多次散射的 VRT，二维非均匀随机介质 VRT 理论，以及在空间微波遥感通道上的各类地表建模与热辐射传输的数值模拟研究。

由合成孔径雷达(SAR) 全极化测量与成像技术的发展，促进了自然地表的全极化散射理论研究，以阐明极化电磁波与复杂地表植被等相互作用的机理和定量分析。第二章讨论了模拟自然植被地表的多层、多成分、非均匀取向非球形粒子全极化散射 Stokes 矢量的 Mueller 矩阵解及其同极化交叉极化散射数值模拟。 作为 Mueller 矩阵解判据和用于 SAR 图像定量分析的相干矩阵理论及其特征值与熵的研究，以及在 SAR 图像分析中的应用。

自然地表如土壤、海面，都是随机粗糙面。第三章讨论了随机粗糙面高阶散射与遮蔽函数的理论,提出用高阶散射相干的角度性变化阐明后向散射增强的理论。模拟强风驱使下海面散射辐射的泡沫散射与双尺度面散射复合模型，以及在海面风场遥感中的应用。

第四章讨论了介电强起伏随机介质与密集粒子散射相干的理论。这是对从能量守恒出发散射独立递加的 VRT 理论的重要修正。该章讨论了模拟冰雪的介电强起伏随机介质与大小分布的密集粒子散射的模拟理论、计算方法与应用。

第五章讨论了空对地定量遥感的数值模拟和星载微波数据验证的研究，提出了多类地表(植被、冰雪、海冰、海风、沙漠、洪涝等) 星载微波成像辐射计（ SSM/I ）遥感数据标定和验证的方法，讨论了主动和被动遥感的相关特征。与星载遥感数据(特别在中国广泛的区域内),作了全面的比较和分析。将区域性地球环境的遥感数值模拟研究、空对地遥感观测数据、及其特征性指数结合起来，发展数据标定验证的新算法，定量地提取和反演大气和地表各种特征性的物理和水文参数时间和空间尺度上的分布和变化。提出了图解网络法、人工神经网络法、指数空间自相关统计法等反演新方法，以及 X 波段散射计辐射计组合系统的研制与实验等。

第六章讨论复杂介质电磁散射理论与计算电磁学方法，包括随机群聚的非球形粒子集合性散射的 T 矩阵数值解；密集颗粒复合介质有效介电特性的计算；手征介质并矢 Green 函数电磁理论，提出用角相关函数在非记忆线上增宽来识别随机粗糙面上散射目标的方法；以及三维体积分方程的快速精确多极子方法等。

自作者回国后的科研工作，始终得到了中国国家自然科学基金委员会地球科学部、信息科学部的大力支持与帮助。作者对其导师、合作者与学生在这些工作中的合作与贡献深致谢意。

“纸上得来终觉浅，绝知此事须躬行”。在新世纪到来之际，作者怀着不敢懈怠的心情，与同志们（特别是青年同志们）一起为祖国现代化的最终实现而竭诚尽责。巴甫洛夫曾说过：“对于科学研究，要有满腔的热情。即使我们有两次生命，那也是不够的”。

Introduction

This book collected some journal papers published by the author with his collaborators during 1980-1999 whilst he was a graduate student for Ph.D. degree in the Massachusetts Institute of Technology, USA and till now he holds professorship in the Fudan University, China. Most of these papers were chosen from the English journals, it should be convenient to the readers in both China and abroad.

This book summarizes the contributions by the author with his collaborators on the areas such as electromagnetic wave scattering, propagation in random media, modeling and simulation for quantitative microwave remote sensing, data validation and parameters retrieval from measurements of satellite-borne remote sensing,, and computational electromagnetics of complex media.It contains six chapters. Each chapter is focus on one topic. The first chapter discusses the vector radiative transfer (VRT) theory for the study of multiple scattering and radiative transfer of polarized electromagnetic intensity-Stokes vector. The VRT theory for modeling of natural media, such as atmospheric precipitation, sea ice, vegetation canopy and land surfaces, etc., and numerical simulation for space-borne microwave remote sensing are developed. The VRT theory for strongly fluctuating, anisotropic random media, and high-dimensional VRT equation are also discussed in this chapter.

Advance of polarimetric measurement and imagery of SAR technology has greatly promoted study of fully polarimetric scattering of the Earth surfaces. Chapter 2 presents simulation of the Mueller matrix solution for multi-layered, multi-components, and non-uniformly oriented, nonspherical scatterers for modeling canopy surfaces. The theory of coherency matrix, eigenvalues and entropy are developed, and are compared with SAR images.

Chapter 3 discusses scattering from randomly rough surface. High-order scattering from rough surface and shadowing function are discussed. Angular enhancement of backscattering is analytically derived. To model sea surface driven by strong winds, a composite model of foam scatterers with two-scale surface approximation is developed, and is applied to active and passive remote sensing of sea surface winds.

Chapter 4 is, especially, devoted to strong fluctuation theory. Scattering coherency from strongly fluctuating media, and dense scatterers are studied. It is an important progress to conventional VRT where independent scattering is usually assumed. This theory is applied to remote sensing of snow fields.

Chapter 5 contains a lot of simulation, data validation and parameter retrieval from satellite-borne remote sensing, such as DMSP SSM/I. Theoretical simulation, measurements and data from remote sensing observation are linked to quantitatively invert information for the Earth surfaces, e.g. vegetation canopy, snow, sea ice, sea surface winds, sand, flooding, etc., and spatial and temporal variations. Correlation of active and passive remote sensing is demonstrated. Some novel retrieval algorithms such as meshed graph, ANN(artificial neural network) method, statistics of spatial auto-correlation etc. are presented. A novel system of combined scatterometer and radiometer at X band and fields experiments are introduced.

Chapter 6 discusses computational electromagnetics of complex media. For example,

the T-matrix solution for collective scattering of clustered non-spherical scatterers, the effective dielectric property of particulate media, electromagnetuics of chiral media and dyadic Green's function, the broadened width of angular correlation function on non-memorial line to detect a target situated over rough surface, the fast multi-pole method of volume integral equation are discussed.

The author greatly appreciates the support from the Divisions of the Earth Science and Information Science of the National Natural Science Foundation of China during his research works in the Fudan University. He is very grateful to his advisors, collaborators and students for their contributions.

目　录
Contents

第三章 随机粗糙面散射理论
Chapter 3 Scattering from Randomly Rough Surface

第四章 强起伏理论与密集粒子散射
Chapter 4 Strong Fluctuation Theory and Scattering from Dense Scatter Media

第五章 遥感模拟、数据验证与反演
Chapter 5 Simulation and Data Validation of Remote Sensing, and Inversion

第六章 复杂介质电磁学与计算

Chapter 6 Electromagnetics of Complex Media and Computational Methods

第一章

随机介质矢量辐射传输理论与遥感建模

Chapter 1

Theory of Vector Radiative Transfer in Random Media for Remote Sensing Modeling

原书空白

1.1

Passive and active remote sensing of atmospheric precipitation

Y. Q. Jin and J. A. Kong

Both passive and active remote sensing of atmospheric precipitation are studied with the vector radiative transfer equations by making use of the Mie scattering phase functions and incorporating the raindrop-size distributions. For passive remote sensing we employ the Gaussian quadrature method to solve for the brightness temperatures. For active remote sensing an iterative approach carrying out to the second order in albedo is used to calculate for the bistatic scattering coefficients, the backscattering cross sections/unit volume, and the interchannel cross talks. The calculated results are plotted as a function of rainfall rates and compared to various available experimental data. The theoretical model is easily applied to the remote sensing of aerosol particles, smoke, fog, and haze at infrared and visible frequencies.

I. Introduction

Electromagnetic wave scattering at visible, infrared, and microwave frequencies by a turbid atmosphere (precipitation, cloud, smoke, haze, fog, etc.) was studied extensively for both passive and active remote sensing.[1–6] The scatterers are generally modeled as spherical Mie scatterers, and the radiative transfer (RT) equations are applied. In passive probing of rain rates the scalar RT theory has been used.[3,4] In active remote sensing of the atmosphere the single-scattering assumption is often used.[7] In scalar RT approaches the assumed Gaussian phase function[6] is proposed, which is based on small angle approximation.

In this paper we apply the vector radiative transfer equation to study both the passive and active remote-sensing problems. The Mie scattering phase function matrix is used and averaged over the raindrop-size distributions to solve for the brightness temperatures and the scattering coefficients. We use the Gaussian quadrature method to solve for the brightness temperatures in passive remote sensing. In active remote sensing all four Stokes parameters (I_v, I_h, U, V) are employed. Every term of the phase function matrix is expressed as a truncated series. We use the iterative approach to the second order in albedo to calculate for the backscattering cross section, bistatic scattering coefficients, and interchannel cross talk.[8] Both the passive and active remote-sensing results are compared with experimental data. The same technique can be applied to the remote probing of atmospheric aerosol, cloud, smoke, haze, and fog at infrared or optical frequencies.

II. Theory for Passive Remote Sensing

Consider a precipitation layer consisting of spherical raindrops with permittivity ε_s, which is calculated by the Debye formula.[10] The layer consists of a distribution of different drop sizes and extends from $z = 0$ to $z = -d$ (Fig. 1). Medium 2 is assumed homogeneous. The radiative transfer equations inside the rain layer take the following forms:

$$\cos\theta \frac{d}{dz}\begin{bmatrix} I_v(\theta,z) \\ I_h(\theta,z) \end{bmatrix} = (\kappa_{ad} + \kappa_{ag})CT_1 - (\kappa_{ed} + \kappa_{ag})\begin{bmatrix} I_v(\theta,z) \\ I_h(\theta,z) \end{bmatrix} + \int_0^{\pi} d\theta' \sin\theta' \begin{bmatrix} (v,v') & (v,h') \\ (h,v') & (h,h') \end{bmatrix}\begin{bmatrix} I_v(\theta',z) \\ I_h(\theta',z) \end{bmatrix}, \quad (1)$$

where $I_v(\theta,z)$ and $I_h(\theta,z)$ are the specific intensities for the vertical and horizontal polarizations, T_1 is the temperature of the raindrops and the atmosphere, $C = K/\lambda^2$ with K denoting the Boltzmann constant and λ the free-space wavelength, $\kappa_{ed} = \kappa_{sd} + \kappa_{ad}$ is the extinction coefficient of raindrops, κ_{sd} and κ_{ad} are the scattering and absorption coefficients, κ_{ag} is the absorption coefficient of atmospheric gases (water vapor and oxygen), $0 < \theta < \pi$, and (v,v'), (v,h'), (h,v'), and (h,h') are the Mie scattering phase functions.[1]

We assume an ocean or land background with temperature T_2. The boundary conditions are, for $0 < \theta < \pi/2$, at $z = 0$

The authors are with MIT Department of Electrical Engineering & Computer Science, Cambridge, Massachusetts 02139.

Received 2 February 1983.
0003-6935/83/172535-11$01.00/0.

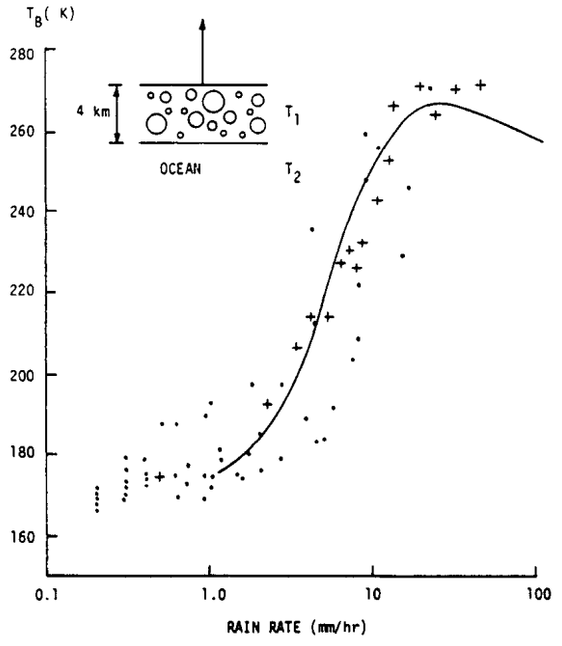

Fig. 1. Geometrical configuration of the problem.

$$\begin{bmatrix} I_v(\pi-\theta,0) \\ I_h(\pi-\theta,0) \end{bmatrix} = 0 \tag{2}$$

and at $z = -d$

$$\begin{bmatrix} I_v(\theta,-d) \\ I_h(\theta,-d) \end{bmatrix} = \begin{bmatrix} r_v(\theta) I_v(\pi-\theta,-d) \\ r_h(\theta) I_h(\pi-\theta,-d) \end{bmatrix} + CT_2 \begin{bmatrix} 1-r_v(\theta) \\ 1-r_h(\theta) \end{bmatrix}, \tag{3}$$

where $r_v(\theta)$ and $r_h(\theta)$ are, respectively, the reflectivities for the vertical and horizontal polarizations.[2]

The brightness temperatures as measured by radiometers are simply

$$\begin{bmatrix} T_{Bv} \\ T_{Bh} \end{bmatrix} = \frac{1}{C} \begin{bmatrix} I_v(\theta,0) \\ I_h(\theta,0) \end{bmatrix} \tag{4}$$

at $z = 0$ and

$$\begin{bmatrix} T_{Bv} \\ T_{Bh} \end{bmatrix} = \frac{1}{C} \begin{bmatrix} I_v(\pi-\theta,-d) \\ I_h(\pi-\theta,-d) \end{bmatrix} \tag{5}$$

at $z = -d$. The task is to solve the radiative transfer Eqs. (1) subject to the boundary conditions (2) and (3).

Numerical solutions are facilitated by replacing the integral in Eq. (1) by Gaussian quadratures[1,7]:

$$\mu_i \frac{d}{dz} \begin{bmatrix} I_v(\theta_i,z) \\ I_h(\theta_i,z) \end{bmatrix} = (\kappa_{ad} + \kappa_{ag}) CT_1 - (\kappa_{ed} + \kappa_{ag}) \begin{bmatrix} I_v(\theta_i,z) \\ I_h(\theta_i,z) \end{bmatrix} + \sum_{j=-N}^{N} a_j \begin{bmatrix} (v_i,v_j) & (v_i,h_j) \\ (h_i,v_j) & (h_i,h_j) \end{bmatrix} \begin{bmatrix} I_v(\theta_j,z) \\ I_h(\theta_j,z) \end{bmatrix}, \tag{6}$$

where $i = \pm 1, \ldots, \pm N$, $\mu_i = \cos\theta_i$, and a_j are the Christoffel numbers. In our calculation we use $N = 6$.

In Figs. 2 and 3 we illustrate the brightness temperatures calculated for an ocean background for a precipitation layer with 4-km thickness. The Marshall-Palmer distribution is used to average over the raindrop-size distributions. We see that both T_{Bv} and T_{Bh} are cold at a small rain rate due to the cold ocean background. As the rain rate increases, the brightness

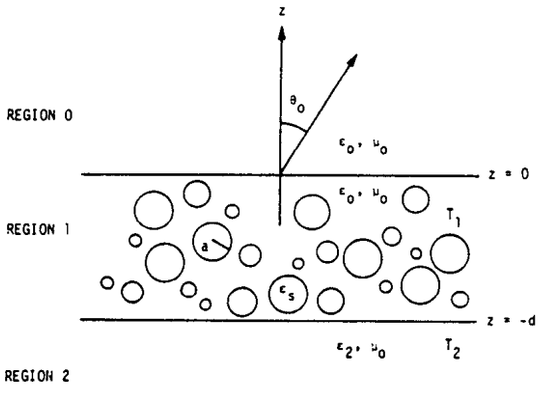

Fig. 2. Brightness temperature vs rain rate at 19.35 GHz. Data given in Ref. 3.

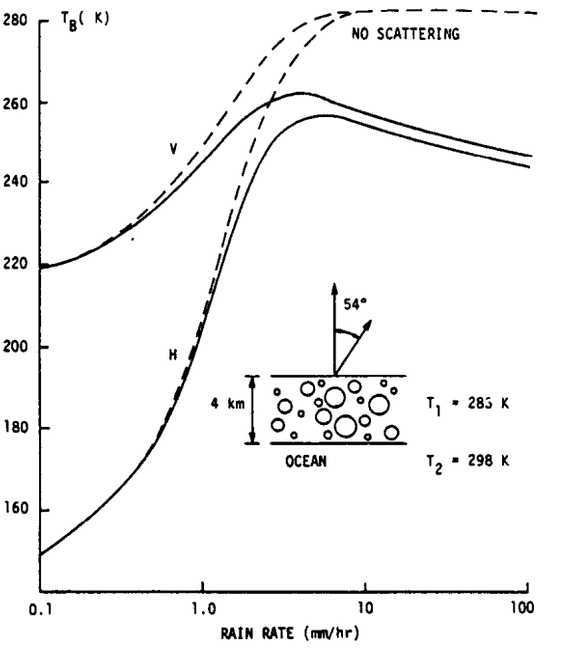

Fig. 3. Brightness temperature vs rain rate at 37 GHz.

temperature increases due to emission from the raindrops. However, compared with the calculation without taking into account the Mie scattering effects as shown with dashed lines, the scattering induces darkening effects, especially at higher rain rates. In Fig. 2 we show that the rainfall model calculations are in good agreement with data collected by Wilheit *et al.*[3] Dots are from simultaneous measurements of the brightness temperatures over ocean by the Nimbus 5 ESMR and the rain rates by the WSR-57 meteorological radar. Crosses are inferred from ground-based measurements of the brightness temperatures and direct measurements of rainfall rates.

III. Theory for Active Remote Sensing

The atmospheric precipitation is modeled as a layer of spherical Mie scatterers with permittivity ε_s and radius a governed by the Laws-Parson distribution, which has been used in most studies of active probing of

rainfall. For active remote sensing the vector radiative transfer equation takes the form[1]

$$\cos\theta \frac{d}{dz}\bar{I}(\theta,\phi,z) = -\kappa_a \bar{I}(\theta,\phi,z) - \kappa_s \bar{I}(\theta,\phi,z) + \int_0^{\pi} d\theta' \sin\theta' \int_0^{2\pi} d\phi' \bar{P}(\theta,\phi;\theta',\phi') \cdot \bar{I}(\theta',\phi',z), \quad (7)$$

where the specific intensity $\bar{I}$ contains all four Stokes parameters

$$\bar{I}(\theta,\phi,z) = \begin{bmatrix} I_v(\theta,\phi,z) \\ I_h(\theta,\phi,z) \\ U(\theta,\phi,z) \\ V(\theta,\phi,z) \end{bmatrix}, \quad (8)$$

$\bar{P}(\theta,\phi;\theta',\phi')$ is the scattering phase-function matrix, and κ_a and κ_s are the absorption and scattering coefficients calculated by the Mie theory incorporating the Laws-Parsons size distribution for atmospheric precipitations.

For a plane wave propagating in the direction θ_{oi},ϕ_{oi} and impinging on a precipitation layer of thickness d we write the boundary conditions at $z = 0$ and $z = -d$ as, for $0 < \theta < \pi/2$,

$$\bar{I}(\pi - \theta,\phi,z = 0) = \bar{I}_{oi}\delta(\cos\theta - \cos\theta_{oi})\delta(\phi - \phi_{oi}), \quad (9a)$$

$$\bar{I}(\theta,\phi,z = -d) = 0. \quad (9b)$$

The bistatic scattering coefficient is defined as the ratio of scatterer power of polarization β/unit solid angle in the direction of θ_s and ϕ_s to the incident power of polarization in the direction θ_{oi} and ϕ_{oi} averaged over 4π rad:

$$\gamma_{\beta\alpha}(\theta_s,\phi_s;\theta_{oi},\phi_{oi}) = 4\pi \frac{I_{s\beta}(\theta_s,\phi_s)\cos\theta_s}{I_{oi\alpha}\cos\theta_{oi}}, \quad (10)$$

where $\alpha,\beta = v$ or h denoting vertical polarization or horizontal polarization, respectively. In the backscattering direction as $\theta_s = \theta_{oi}$ and $\phi_{os} = \pi + \phi_{oi}$, the backscattering cross section/unit area is defined as

$$\sigma^0_{\beta\alpha}(\theta_{oi}) = \cos\theta_{oi}\gamma_{\beta\alpha}(\theta_{oi},\pi + \phi_{oi};\theta_{oi},\phi_{oi}) = 4\pi\cos\theta_{oi}\frac{I_{oi\beta}(\theta_{oi},\pi + \phi_{oi})}{I_{oi\alpha}}. \quad (11)$$

The backscattering cross section/unit volume $\sigma_{\beta\alpha}$ is obtained by dividing $\sigma^0_{\beta\alpha}$ by the layer thickness d.

Another parameter that is of importance in the communications applications is the cross talk CX defined as the ratio of the power received through the offset channel to that through the direct channel. The total power in the line-of-sight direct channel is equal to the sum of the coherent and incoherent intensities

$$P_t = I_o \exp(-\kappa_e d \sec\theta_i) + \int_{\Omega_r} d\Omega' I_s(\pi - \theta',\phi') \approx I_o \exp(-\kappa_e d \sec\theta_i) + I_s(\pi - \theta_i,\phi_i,-d)\cdot\Omega_r. \quad (12)$$

The scattered power as received by the offset channel is

$$P_s = \int_{\Omega_r} d\Omega' I_s(\pi - \theta_s',\phi_s') \approx I_s(\pi - \theta_s,\phi_s,-d)\cdot\Omega_r, \quad (13)$$

where it is assumed that I_s is uniform over a very narrow radiant angle Ω_r of the antenna. The cross talk is defined as

$$CX = \frac{P_s}{P_t} = \frac{I_s(\pi - \theta_s,\phi_s,-d)\cdot\Omega_r}{I_o \exp(-\kappa_e d \sec\theta_i) + I_s(\pi - \theta_i,\phi_i,-d)\cdot\Omega_r}. \quad (14)$$

Notice that[11] $\Omega_r \approx \pi(\theta_{hr}/2)^2$ and $\theta_{hr} \approx \pi^2/G$ is the half-power beamwidth of the receiving antenna with gain G, where G is assumed to be 40 dB in our calculations.

IV. Iterative Approach

A. Iterative Procedure

When absorption is dominant over scattering, we can obtain closed-form solutions by using an iterative approach using the albedo (κ_s/κ_e) as the small parameter to carry out perturbation analysis. First, we break up the intensities in the scattering layer into backward propagating intensities $\bar{I}(\theta,\phi,z)$ and forward propagating intensities $\bar{I}(\pi - \theta,\phi,z)$ for $0 < \theta < \pi/2$. We then incorporate the boundary conditions to obtain the following integral equations:

$$\bar{I}(\theta,\phi,z) = \sec\theta \exp(-\kappa_e z \sec\theta) \int_{-d}^{z} dz' \exp(\kappa_e z' \sec\theta) \times \int_0^{\pi/2} d\theta' \sin\theta' \int_0^{2\pi} d\phi' \{\bar{P}(\theta,\phi;\theta',\phi')\cdot\bar{I}(\theta',\phi',z') + \bar{P}(\theta,\phi;\pi - \theta',\phi')\bar{I}(\pi - \theta',\phi',z')\}, \quad (15a)$$

$$\bar{I}(\pi - \theta,\phi,z) = \bar{I}_{oi}\delta(\cos\theta_o - \cos\theta_{oi})\delta(\phi_o - \phi_{oi})\exp(\kappa_e z \sec\theta) + \sec\theta \exp(\kappa_e z \sec\theta) \int_z^0 dz' \exp(-\kappa_e z' \sec\theta) \int_0^{\pi/2} d\theta' \sin\theta' \times \int_0^{2\pi} d\phi' \{\bar{P}(\pi - \theta,\phi;\theta',\phi')\cdot\bar{I}(\theta',\phi',z') + \bar{P}(\pi - \theta,\phi;\pi - \theta',\phi') \times \bar{I}(\pi - \theta',\phi',z')\}, \quad (15b)$$

where the first term of Eq. (15b) is the incident intensity in the θ_{oi},ϕ_{oi} direction. The zeroth-order solution takes the form

$$\bar{I}^{(0)}(\theta,\phi,z) = 0, \quad (16a)$$

$$\bar{I}^{(0)}(\pi - \theta,\phi,z) = \bar{I}_{oi}\delta(\cos\theta_o - \cos\theta_{oi}) \times \delta(\phi_o - \phi_{oi})\exp(\kappa_e z \sec\theta). \quad (16b)$$

The first-order solutions are found to be

$$\bar{I}^{(1)}(\theta,\phi,z) = \exp(-\kappa_e z \sec\theta)\sec\theta\bar{P}(\theta,\phi;\pi - \theta_i,\phi_i)\cdot\bar{I}_{oi} \times \frac{\exp[\kappa_e z(\sec\theta + \sec\theta_i)] - \exp[-\kappa_e d(\sec\theta + \sec\theta_i)]}{\kappa_e(\sec\theta + \sec\theta_i)}, \quad (17a)$$

$$\bar{I}^{(1)}(\pi - \theta,\phi,z) = -\exp(\kappa_e z \sec\theta)\sec\theta\bar{P}(\pi - \theta,\phi;\pi - \theta_i,\phi_i)\cdot\bar{I}_{oi} \times \frac{1 - \exp[-\kappa_e z(\sec\theta - \sec\theta_i)]}{\kappa_e(\sec\theta - \sec\theta_i)}. \quad (17b)$$

The corresponding first-order scattered intensities are, in region 0,

$$\bar{I}^{(1)}_o(\theta_{os},\phi_{os}) = \bar{I}^{(1)}(\theta_s,\phi_s,z = 0) = \sec\theta_s\bar{P}(\theta_s,\phi_s;\pi - \theta_i,\phi_i) \times \bar{I}_{oi}\frac{1 - \exp[-\kappa_e d(\sec\theta_s + \sec\theta_i)]}{\kappa_e(\sec\theta_s + \sec\theta_i)} \quad (18a)$$

and in region 2

$$\bar{I}_2^{(1)}(\pi-\theta_{2s},\phi_{2s}) = \bar{I}^{(1)}(\pi-\theta_s,\phi_s,z=-d)$$
$$= -\exp(-\kappa_e d\sec\theta_s)\sec\theta_s$$
$$\bar{P}(\pi-\theta_s,\phi_s,\pi-\theta_i,\phi_i)\cdot\bar{I}_{oi}$$
$$\cdot\frac{1-\exp[\kappa_e d(\sec\theta_s-\sec\theta_i)]}{\kappa_e(\sec\theta_s-\sec\theta_i)}. \tag{18b}$$

It is noted that, in the first-order solutions, the cross-polarization contributions are zero, and we must carry the iterative process to at least the second order to account for the depolarization effects.

The second-order solutions in region 0 in the direction $(\phi_{os},\pi+\phi_{os})$ are

$$\bar{I}_o^{(2)}(\theta_{os},\pi+\phi_{os}) = \sec\theta_s\int_0^{\pi/2}d\theta'\sin\theta'$$
$$\times\int_0^{2\pi}d\phi'\{\bar{P}(\theta_s,\pi+\phi_s;\theta',\phi')$$
$$\times\bar{A}_1(\theta',\phi')+\bar{P}(\theta_s,\pi+\phi_s;\pi-\theta',\phi')\cdot\bar{A}_2(\theta',\phi')\}, \tag{19a}$$

where

$$\bar{A}_1(\theta',\phi') = \int_{-d}^{0}dz'\exp(\kappa_e z'\sec\theta_i)\bar{I}^{(1)}(\theta',\phi',z')$$
$$= \sec\theta'\cdot\bar{P}(\theta',\phi';\pi-\theta_i,\phi_i)\cdot\bar{I}_{oi}\cdot\frac{1}{\kappa_e(\sec\theta'+\sec\theta_i)}$$
$$\times\{D_2(\theta_s,\theta_i)-D_1(\theta_s,\theta')\exp[-\kappa_e d(\sec\theta'+\sec\theta_i)]\}, \tag{19b}$$

$$\bar{A}_2(\theta',\phi') = \int_{-d}^{0}dz'\exp(\kappa_e z'\sec\theta_i)\exp(\kappa_e z'\sec\theta')$$
$$\times\sec\theta'\cdot\bar{P}(\pi-\theta',\phi';\pi-\theta_i,\phi_i)$$
$$\times\bar{I}_{oi}\cdot\frac{-1}{\kappa_e(\sec\theta'-\sec\theta_i)}\cdot\{1-\exp[-\kappa_e z'(\sec\theta'-\sec\theta_i)]\}$$
$$= \sec\theta'\cdot\bar{P}(\pi-\theta',\phi';\pi-\theta_i,\phi_i)\cdot\bar{I}_{oi}\cdot\frac{-1}{\kappa_e(\sec\theta'-\sec\theta_i)}$$
$$\times[D_2(\theta_s,\theta')-D_2(\theta_s,\theta_i)], \tag{19c}$$

$$D_1(\theta_i,\theta_s) = \frac{1-\exp[-\kappa_e d(\sec\theta_i-\sec\theta_s)]}{\kappa_e(\sec\theta_i-\sec\theta_s)}, \tag{19d}$$

$$D_2(\theta_s,\theta_i) = \frac{1-\exp[-\kappa_e d(\sec\theta_s+\sec\theta_i)]}{\kappa_e(\sec\theta_s+\sec\theta_i)}. \tag{19e}$$

B. Backscattering and Bistatic Scattering Coefficients

We consider a vertically polarized incident wave and calculate the vertical and horizontal polarized scattered intensities to the second order in the iterative process. Using Eq. (19) we obtain

$$\bar{I}_{osv}^{(2)}(\theta_{os},\pi+\phi_{os}) = I_{oiv}\sec\theta_s\cdot\int_0^{\pi/2}d\theta'\sin\theta'\int_0^{2\pi}d\phi'\sec\theta'$$
$$\times\{[P_{11}(\theta_s,\pi+\phi_s;\theta',\phi')\cdot K_1(\theta',\phi')+P_{11}(\theta_s,\pi+\phi_s;\pi-\theta',\phi')$$
$$\times L_1(\theta',\phi')]+[P_{12}(\theta_s,\pi+\phi_s;\theta',\phi')\cdot K_2(\theta',\phi')$$
$$+P_{12}(\theta_s,\pi+\phi_s;\pi-\theta',\phi')\cdot L_2(\theta',\phi')]$$
$$+[P_{13}(\theta_s,\pi+\phi_s;\theta',\phi')\cdot K_3(\theta',\phi')+P_{13}(\theta_s,\pi+\phi_s;\pi-\theta',\phi')$$
$$\times L_3(\theta',\phi')]+[P_{14}(\theta_s,\pi+\phi_s;\theta',\phi')\cdot K_4(\theta',\phi')$$
$$+P_{14}(\theta_s,\pi+\phi_s;\pi-\theta',\phi')\cdot L_4(\theta',\phi')]\}, \tag{20}$$

where

$$K_1(\theta',\phi') = P_{11}(\theta',\phi';\pi-\theta_i,\phi_i)\frac{1}{\kappa_e(\sec\theta'+\sec\theta_i)}$$
$$\times\{D_2(\theta_s,\theta_i)-D_1(\theta_s,\theta')\exp[-\kappa_e d(\sec\theta'+\sec\theta_i)]\}, \tag{21a}$$

$$K_2(\theta',\phi') = P_{21}(\theta',\phi';\pi-\theta_i,\phi_i)\frac{1}{\kappa_e(\sec\theta'+\sec\theta_i)}$$
$$\times\{D_2(\theta_s,\theta_i)-D_1(\theta_s,\theta')\exp[-\kappa_e d(\sec\theta'+\sec\theta_i)]\}, \tag{21b}$$

$$K_3(\theta',\phi') = P_{31}(\theta',\phi';\pi-\theta_i,\phi_i)\frac{1}{\kappa_e(\sec\theta'+\sec\theta_i)}$$
$$\times\{D_2(\theta_s,\theta_i)-D_1(\theta_s,\theta')\exp[-\kappa_e d(\sec\theta'+\sec\theta_i)]\}, \tag{21c}$$

$$K_4(\theta',\phi') = P_{41}(\theta',\phi';\pi-\theta_i,\phi_i)\frac{1}{\kappa_e(\sec\theta'+\sec\theta_i)}$$
$$\times\{D_2(\theta_s,\theta_i)-D_1(\theta_s,\theta')\exp[-\kappa_e d(\sec\theta'+\sec\theta_i)]\}, \tag{21d}$$

$$L_1(\theta',\phi') = P_{11}(\pi-\theta',\phi';\pi-\theta_i,\phi_i)\cdot\frac{-1}{\kappa_e(\sec\theta'-\sec\theta_i)}$$
$$\times[D_2(\theta_s,\theta')-D_2(\theta_s,\theta_i)], \tag{22a}$$

$$L_2(\theta',\phi') = P_{21}(\pi-\theta',\phi';\pi-\theta_i,\phi_i)\cdot\frac{-1}{\kappa_e(\sec\theta'-\sec\theta_i)}$$
$$\times[D_2(\theta_s,\theta')-D_2(\theta_s,\theta_i)], \tag{22b}$$

$$L_3(\theta',\phi') = P_{31}(\pi-\theta',\phi';\pi-\theta_i,\phi_i)\cdot\frac{-1}{\kappa_e(\sec\theta'-\sec\theta_i)}$$
$$\times[D_2(\theta_s,\theta')-D_2(\theta_s,\theta_i)], \tag{22c}$$

$$L_4(\theta',\phi') = P_{41}(\pi-\theta',\phi';\pi-\theta_i,\phi_i)\cdot\frac{-1}{\kappa_e(\sec\theta'-\sec\theta_i)}$$
$$\times[D_2(\theta_s,\theta')-D_2(\theta_s,\theta_i)]. \tag{22d}$$

$P_{ij}(\theta,\phi,\theta',\phi')$ is the term of $\bar{P}(\theta,\phi;\theta',\phi')$ $(i,j=1,2,3,4)$. Its expressions are given in Appendix A. Note that as $\theta'\to\theta_i$,

$$\lim_{\theta'\to\theta_i}\frac{-1}{\kappa_e(\sec\theta'-\sec\theta_i)}[D_2(\theta_s,\theta')-D_2(\theta_s,\theta_i)] = \frac{1}{\kappa_e(\sec\theta_s+\sec\theta_i)}$$
$$\times\{D_2(\theta_s,\theta_i)-D_1(\theta_s,\theta_i)\cdot\exp[-\kappa_e d(\sec\theta_s+\sec\theta_i)]\}. \tag{23}$$

Thus we can obtain the backscattering cross section

$$\sigma_{vv} = 4\pi\cos\theta_{oi}\frac{I_{osv}^{(1)}(\theta_i,\pi+\phi_i)+I_{osv}^{(2)}(\theta_i,\pi+\phi_i)}{I_{oiv}}, \tag{24}$$

and we can obtain the horizontal polarized scattered intensities

$$\bar{I}_{osh}^{(2)}(\theta_{os},\pi+\phi_{os}) = I_{oiv}\sec\theta_s\cdot\int_0^{\pi/2}d\theta'\sin\theta'\int_0^{2\pi}d\phi'\sec\theta'$$
$$\times\{[P_{21}(\theta_s,\pi+\phi_s;\theta',\phi')\cdot K_1(\theta',\phi')+P_{21}(\theta_s,\pi+\phi_s;\pi-\theta',\phi')$$
$$\times L_1(\theta',\phi')]+[P_{22}(\theta_s,\pi+\phi_s;\theta',\phi')\cdot K_2(\theta',\phi')$$
$$+P_{22}(\theta_s,\pi+\phi_s;\pi-\theta',\phi')\cdot L_2(\theta',\phi')]$$
$$+[P_{23}(\theta_s,\pi+\phi_s;\theta',\phi')\cdot K_3(\theta',\phi')+P_{23}(\theta_s,\pi+\phi_s;\pi-\theta',\phi')$$
$$\times L_3(\theta',\phi')]+[P_{24}(\theta_s,\pi+\phi_s;\theta',\phi')\cdot K_4(\theta',\phi')$$
$$+P_{24}(\theta_s,\pi+\phi_s;\pi-\theta',\phi')\cdot L_4(\theta',\phi')]\}. \tag{25}$$

Thus the bistatic scattering coefficient $\gamma_{ohv}(\theta_{os},\pi+\phi_{os};\theta_{oi},\phi_{oi})$ in region 0 is

$$\gamma_{ohv}(\theta_{os}\phi_{os};\theta_{oi},\phi_{oi}) = 4\pi\frac{\cos\theta_s I_{osh}(\theta_s,\phi_s)}{\cos\theta_{oi}I_{oiv}}$$
$$= 4\pi\sec\theta_s\cdot P_{21}(\theta_s,\pi+\phi_s;\pi-\theta_i,\phi_i)\cdot D_2(\theta_s,\theta_i)$$
$$+4\pi\sec\theta_s\int_0^{\pi/2}d\theta'\sin\theta'\sec\theta'\cdot[F_1(\theta_s,\theta')+F_2(\theta_s,\theta')$$
$$+F_3(\theta_s,\theta')+F_4(\theta_s,\theta')], \tag{26}$$

where